Chapter 2

Bubble Rise Phenomena in Non-Newtonian Crystal Suspensions

N.M.S. Hassan, M.M.K. Khan and M.G. Rasul

Additional information is available at the end of the chapter

http://dx.doi.org/10.5772/53760

1. Introduction

1.1. Bubble trajectory

The characteristics of bubble motion in non-Newtonian liquids are still not well understood because many parameters influence the terminal rise velocity, trajectory and shape of bubbles (Frank, 2003). As the bubble motion is a complex problem, the degree of the complexity increases with bubble size (Kulkarni and Joshi, 2005). When bubble rises through liquid, the most resistance will be imposed directly on top and the bubble first moves along a straight vertical path and then develops a zigzag motion which consequently can change into a spiralling motion, at the same incidence as the preceding zigzag (Ellingsen and Risso, 2001; Mougin and Magnaudet, 2002; Shew and Pinton, 2006; Zenit and Magnaudet, 2009).

In most reported studies, very small bubbles (less than 1 mm) rise through water maintaining their spherical shape due to surface tension. The trajectory of these bubbles follows a straight line until it completes its journey (Clift *et al.,* 1978; Duineveld, 1995). On the other hand, considerable deformations are observed for bubbles with diameters larger than 1 mm (Ellingsen and Risso, 2001). This deformation occurs due to the increase in the variations of hydrostatic and dynamic pressure over the bubbles' surface (Magnaudet and Eames, 2000). Therefore, large bubbles cannot remain spherical and deform into oblate spheroids first and then become ellipsoidal, and with further increase in size they switch into a spherical or ellipsoidal cap. Bubble motion such as velocity and trajectory also change with the increase in bubble size (Hassan *et al.,* 2010a).

The bubble is not always rising in straight path. When the bubble size increases, a straight path turns into zigzag or spiral in fluids of small Morton number. Then the path becomes nearly straight again for a spherical cap bubble. Only a straight path is observed (Yang,

2006) in liquids of large Morton number. Aybers and Tapucu (1969) reported different types of trajectories such as zigzag, helical or spiral and rocking motions. Haberman and Morton (1954) also observed rectilinear ($\mathrm{Re} < 300$), spiral and rocking motions. They indicated that the spiral path could be either clockwise or counter-clockwise, depending on the conditions of bubble release. The major axis of the bubble is always directed perpendicular to the direction of motion. Saffman (1956) observed only zigzag bubble rise motions as the bubble rises in water when the radius of the bubble was less than 1 mm, but bubbles of larger radius showed either zigzag or spiral motions. Feng and Leal (1997) verified various possible trajectories for different shape regimes. A single bubble can follow a zigzag path at $\mathrm{Re} \approx 600$, accompanied with vortex shedding behind the bubble. Under the same experimental conditions, Yoshida and Manasseh (1997) reported that the bubbles can also follow a spiral trajectory without vortex shedding. Tsuge and Hibino (1997) reported that the trajectories of rising spherical and ellipsoidal gas bubbles at higher Reynolds numbers are identical.

The trajectories of bubbles are strongly influenced by the bubble deformations and the surrounding fluid flow (Ellingsen and Risso, 2001). Bubble deformations and fluid flow could be explained with dimensionless groups such as the Reynolds Number (Re), the Weber number (We), the Morton number (Mo) and bubble aspect ratio (E) (Hassan *et al.*, 2008c; Hassan *et al.*, 2010a). In fluid mechanics, Re gives a measure of the ratio of inertial forces to viscous forces and consequently quantifies the relative importance of these two types of forces for given flow conditions. On the other hand, We is often useful in analyzing fluid flows where there is an interface between two different fluids, especially for multiphase flows such as bubble rise in liquids. It can be thought of as a measure of the relative importance of the fluid's inertia compared to its surface tension. The quantity is useful in analyzing the formation of droplets and bubbles. The dimensionless number such as Mo, is also used together with the Eötvös number (Eo) to characterize the shape of bubbles or drops moving in a surrounding fluid or continuous phase. Eötvös number is considered as proportional to buoyancy force divided by surface tension force. Theses dimensionless groups are defined as:

$$\mathrm{Re} = \frac{\rho_{liq} d_{eq} U_b}{\mu_1} \tag{1}$$

$$We = \frac{\rho_{liq} U_b^2 d_{eq}}{\sigma} \tag{2}$$

$$Mo = \frac{g \mu_{liq}^4 \Delta\rho}{\rho_{liq}^2 \sigma^3} \tag{3}$$

$$E = \frac{d_w \text{ or semi major axis}}{d_h \text{ or semi minor axis}} \tag{4}$$

Where U_b is the bubble rise velocity, m/sec; d_{eq} is the bubble equivalent diameter, m; ρ_{liq} is the density of the liquid, kg/m^3 ; μ_1 is the liquid viscosity, Pa.s; σ is the surface tension of the liquid, N/m; g is the aacceleration due to gravity, m/s^2 and $\Delta\rho$ is the density difference between liquid and air bubble, kg/m^3.

Usually, Re controls the liquid flow regime around the bubble and We, Mo and E characterise the bubble deformations and bubble shapes. Therefore, the influences of Re, We and Mo are seen as important for elucidation of the bubble trajectories.

Several studies on the behaviour of bubble rise trajectories in water are available in the literature (Haberman and Morton 1954; Saffman 1956; Ellingsen and Risso, 2001; Duineveld, 1995). However, no study exists on bubble trajectories in non-Newtonian crystal suspensions. This study explores the characteristics of the bubble trajectory in non-Newtonian crystal suspensions and compares these results with water and different concentration polymeric solutions.

1.2. Bubble shapes

The shape of the bubbles greatly influences the bubble rise velocity and it has a significant role in determining the rates of heat and mass transfer and coalescence. Normally, a motionless bubble has a spherical shape because surface tension minimises surface area for a given volume. When a bubble has motion, different forces exist such as drag caused by the liquid, viscosity of the liquid, pressure difference between the top and bottom of the bubble as well as the wall effects.

Mainly, three types of shape such as spherical, ellipsoidal and spherical-cap or ellipsoidal cap in free motion under the influence of gravity are observed in Newtonian liquids.

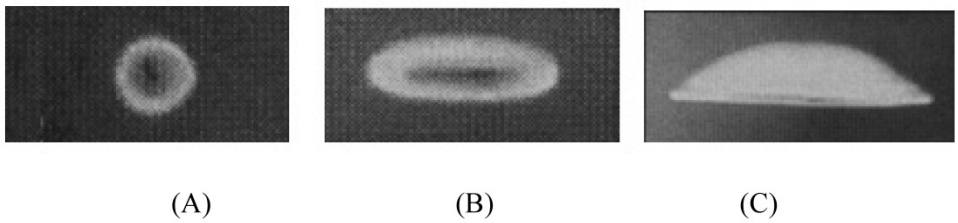

Figure 1. Different types of bubble shape in Newtonian fluid

The shapes of bubble are related to the Re. At low Re, the bubble retains its shape as a sphere because interfacial forces and viscous forces are much more important than inertia forces. Most bubbles of small size fall into this category. The spherical shape of the bubble is shown in the Figure 1(A).

The next category of bubbles is termed “ellipsoidal”; these are oblate with a convex interface around the surface when viewed from the inside. The liquid viscosity may affect the bubble shape, stretching the bubble out laterally, so that actual shapes may differ considerably from

true ellipsoids. However, the general shape is comparable to an ellipsoid which is shown in Figure 1 (B).

Large bubbles have a flat base or a spherical wedge, which may look very similar to segments cut from a sphere. They are heavily distorted from the equilibrium shape of a sphere. In this case, the Reynolds number is high and these bubbles are termed as spherical-cap or ellipsoidal-cap. This type of bubble is shown in Figure 1 (C).

Beside these shapes, some other shapes are also noted in the literature (Clift *et al.,* 1978). A bubble that has an indentation at the rear is known as dimpled. Large spherical or ellipsoidal-caps may also trail thin envelopes of dispersed fluid referred to as skirts. Bubbles in different shape regimes are shown in Figure 2.

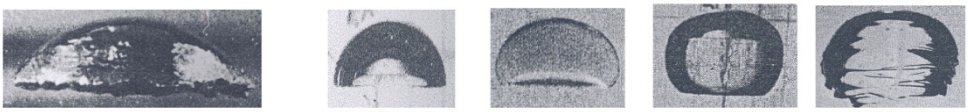

Figure 2. Photograph of bubbles in different shape regime (Clift *et al.,* 1978)

In non-Newtonian liquids, many more shapes of bubble have been reported (Calderbank, 1967; De Kee *et al.,* 1996; Chhabra, 2006). Among those, a distinctive feature of bubble shapes observed in non-Newtonian liquids is the appearance of a "pointed" tail prior to the transition to hemispherical caps. Experimental observations were reported by De Kee and Chhabra (1988) and De Kee *et al.* (1990) in aqueous carboxyl-methylcellulose and polyacrylamide solutions that had bubble shapes changing from spherical to prolate tear drop, then to oblate cusped, to oblate and finally to Taylor-Davies (Davies and Taylor, 1950) type spherical caps with the increase of bubble size. Shape behaviours also depend on the rheological and physical properties of the liquid. A large number of different shapes are observed in rheologically complex liquids depending upon the physical properties of the dispersed and continuous phases and the size of bubbles.

1.2.1. Bubble shapes in Newtonian fluids

It is usually established that the shapes of the bubbles rising in Newtonian fluid can be generalized in terms of the magnitudes of the following dimensionless parameters (Grace, 1973, Grace *et al.,* 1976; Clift *et al.,* 1978; Chhabra, 2006) such as Re, Eo, Mo, viscosity ratio, $X = \dfrac{\mu_a}{\mu_{liq}}$, and density ratio, $\gamma = \dfrac{\rho_a}{\rho_{liq}}$.

For the case of a bubble with a negligible inner density, the Mo as defined in equation (3) can be simplified to:

$$Mo = \frac{g\mu_{liq}^4}{\rho_{liq}^2 \sigma^3} \tag{5}$$

Based on these dimensionless groups, researchers (Grace *et al.,* 1976; Bhaga, 1976; Bhaga and Weber, 1981; Grace and Wairegi, 1986) have constructed the so called "shape maps" as shown in Figure 3.

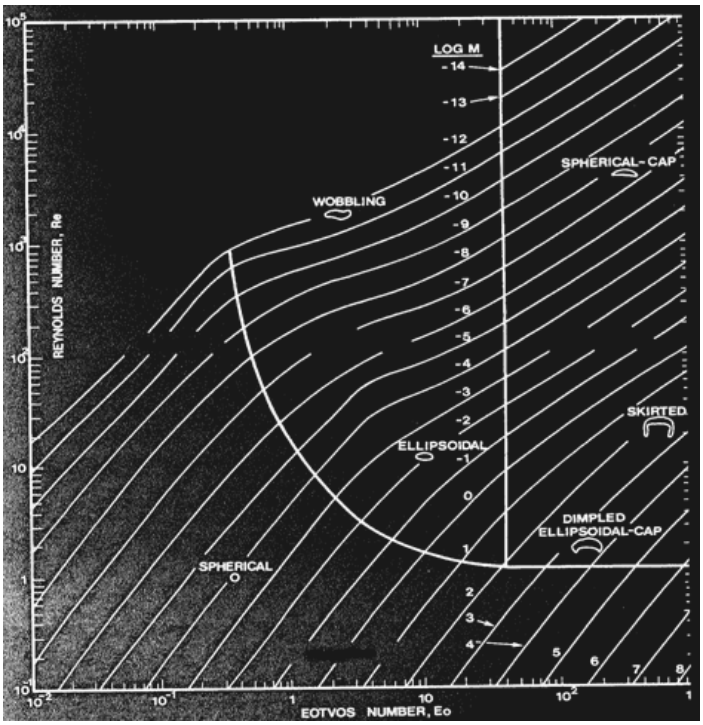

Figure 3. Shape regimes for bubbles (Clift *et al*., 1978)

This map is a quite useful qualitative method in measuring the shapes of bubbles for Newtonian liquids, based on visual observations. The shape changes from one form to another in which usually occurs over a range of conditions in comparison to the sharp boundaries shown in all such maps (Chhabra, 2006). Spherical shape is observed at very small values of Mo, Eo and Re but on the other hand, ellipsoidal bubbles are encountered at relatively high Re and moderate Eo. Finally, the spherical cap shape occurs only at moderately high Eo and Re. Furthermore, Tadaki and Maeda (1961) developed a simple quantitative shape map which has also proved to be very successful for computing the bubbles shapes in Newtonian liquids. This approach incorporates eccentricity (E) which is defined as the maximum width of the bubble divided by the maximum height of the bubble.

1.2.2. Bubble shapes in non-Newtonian fluids

Many investigators have presented the quantitative information on bubble shapes in non-Newtonian fluids (Carreau *et al*., 1974; De Kee and Chhabra, 1988; Miyahara and Yamanaka,

1993; De Kee *et al.*, 1996; Chhabra, 2006). It is found that bubbles rising in stagnant non-Newtonian inelastic and viscoelastic fluids remain spherical in shape up to larger volumes than in Newtonian media (De Kee and Chhabra, 1988; De Kee *et al*., 1986, 1996, 2002). For predicting the bubble shapes in non-Newtonian fluids, the quantitative approach involved with eccentricity is found more useful compared to qualitative (shape maps) approach. General observations of the shape of the bubbles shows that the bubbles moving in non-Newtonian fluids are tear drop shaped at small Re in viscoelastic liquids. It is reported that the bubble shapes tend to be spherical, oblate spheroidal and finally spherical capped with increasing Re . The quantitative description of the bubble shapes in terms of the process and rheological parameters can be seen in terms of an eccentricity (E) or aspect ratio defined as the ratio of the maximum width to the maximum height. Literature suggests that prolate shaped ($E < 1$) and oblate shaped ($E > 1$) bubbles should be treated separately (Acharya *et al.*, 1977). A quantitative relationship between the bubble eccentricity and the relevant dimensionless groups has been attempted by Miyahara and Yamanaka (1993).

Again, a new dimensionless group G_1 which is a measure of the ratio of the elastic stresses to surface tension stresses can be simplified (Acharya *et al*., 1977) as:

$$G_1 = \frac{K\left(\frac{U_b}{R}\right)^n}{\sigma R} \tag{6}$$

The aspect ratio (E < 1) for prolate shaped bubbles correlated empirically with this new dimensionless group G_1 as:

$$E = 0.616(G_1)^{-0.168} \tag{7}$$

The above correlation (7) could be used at least in the range of $0.68 < E < 1$.

At large bubble volumes or high Reynolds numbers, when the bubble moves in Newtonian fluid tending to make the bubble shape an oblate spheroid (E >1), the fluid inertia causes major distortions from sphericity. The tendency towards distortion is opposed by surface tension stresses. In this region, We can be defined as the ratio of the internal stresses to the surface tension stresses; this controls the bubble deformation. In this context for high Reynolds number flow, another new dimensionless group G_2 has been simplified (Acharya *et al*., 1977).

$$G_2 = \frac{Wi}{\mathrm{Re}\,We} \tag{8}$$

The Weissenberg number (Wi) is defined by:

$$Wi = \dot{\gamma}\lambda \quad (\text{Shear rate * relaxation time}) \tag{9}$$

The aspect ratio correlated empirically with the G_2 for oblate shaped bubble is given by:

$$E = 1 + 0.00083 G_2^{-0.87} \tag{10}$$

Equation (10) applies over the range of variables $1 \le E \le 1.5$ and $0.001 \le G_2 \le 0.015$.

For Newtonian and non-Newtonian fluids, bubble diameter (width and height) and eccentricity are determined experimentally and this experimental data are used for the calculation of different dimensional groups. Bubble shapes in Newtonian fluids can be predicted in comparison with the so called "shape maps". At the end, different theoretical bubble shapes are computed in comparison with above correlation and data from the relevant literature.

1.3. Path and shape instability of a rising bubble

The path instability of a bubble is a fascinating phenomenon of bubble trajectory when bubble rises in fluids (Hassan *et al.,* 2010a). It is one of the most challenging and least understood aspects of bubble dynamics (Magnaudet and Eames, 2000). Many researchers have investigated experimentally and numerically the path instability of bubbles (Haberman and Morton, 1954; Saffman, 1956; Aybers and Tapucu, 1969; Wegener and Parlange, 1973; Mougin and Magnaudet, 2002; Mougin and Magnaudet, 2006; Brenn *et al.,* 2006; Yang and Prosperetti, 2007; Zenit and Magnaudet, 2008; Fernandes *et al.,* 2008; Adoua *et al.,* 2009, Hassan *et al.,* 2010a). Many investigators (Haberman and Morton, 1954; Saffman, 1956; Aybers and Tapucu, 1969; Duineveld, 1994, 1995; Maxworthy, 1996; de Vries, 2001; de Vries *et al.,* 2002) indicated that the onset of path instability of a bubble is in general occurring at different stages, and the condition for bubble deformation is that We must exceed a critical value ($We > We_{cr}$). Duineveld (1994) determined that the critical We at which a bubble starts to change its path is in the range $We_{cr} \approx 3.3$ in clean water. Saffman (1956) observed the onset of path instability in water occurs once the equivalent bubble diameter d_{eq} is 1.4 mm for a straight path, $1.4\ mm \le d_{eq} \le 2.0\ mm$ for a zigzag trajectory, and $d_{eq} = 2.0\ mm$ for both zigzag and spiral trajectories, and also estimated the corresponding critical Re to be $\mathrm{Re}_{cr} \simeq 400$ for path instability. Aybers and Tapucu (1969) indicated a rectilinear path at the equivalent diameter of $d_{eq} = 1.34\ mm$, a spiral trajectory for $1.34\ mm \le d_{eq} \le 2.0\ mm$, zigzag trajectory changing to helical trajectory for $2.0\ mm \le d_{eq} \le 3.60\ mm$, and only zigzag trajectory for $3.60\ mm \le d_{eq} \le 4.2\ mm$. The onset of path instability is generally assumed to occur at a critical Weber number (Duineveld, 1994; Maxworthy, 1996 and Tsuge and Hibino, 1997). Tsuge and Hibino (1997) proposed an empirical relation for determining We_{cr} which is presented in equation (11).

The shape of a bubble is also an important variable for predicting the bubble rise characteristics and it also depends on dimensionless groups We (Churchill, 1989) as the bubble rise velocity, U_b. The bubble shape is assumed to be stable for low We and becomes unstable for larger We. Therefore, the We is an important parameter to determine the bubble deformation. Many investigators (Haberman, 1954; Saffman,1956; Hartunian and

Sears, 1957; Aybers and Tapucu,1969; Duineveld, 1995) indicated that the onset of both shape and path instability of a bubble are in general occurring at different stages, and the condition for bubble deformation is that We exceeds a critical value ($We > We_{cr}$). The literature suggests that the critical We at which a bubble starts to deform is in the range, $We_{cr} \approx 3\ to\ 4$ (Saffman, 1956). Deane and Stokes (2002) indicated that $We_{cr} = 4.7$ must be exceeded for the deformation of the bubble to occur, and they found the critical Reynolds number $\mathrm{Re}_{cr}(450)$ that must be exceeded for bubble shape oscillations and elongation and subsequent deformation to occur in water. Tsuge and Hibino (1997) proposed an empirical relation for determining We_{cr} as:

$$We_{cr} = 21.5\mathrm{Re}_{cr}^{-0.32}, \qquad \mathrm{Re}_{\mathrm{cr}} = 9.0Mo^{-0.173} \tag{11}$$

Churchill (1989) and Chhabra (2006) indicated that the shape of the bubble is also represented quantitatively by the aspect ratio or eccentricity ratio and is given by:

$$E = \frac{d_w \ or\ major\ axis\ diameter}{d_h \text{ or minor axis diameter}} \tag{12}$$

Moreover, bubble deformation is accurately measured by the deformation parameter, D regardless of any liquid medium (Whyte *et al.*, 2000) which is given by:

$$D = \frac{d_w - d_h}{d_w + d_h} \tag{13}$$

The literature indicates that the path and shape instability is well understood in water as well as some non-Newtonian fluids. As there is no massecuite data available for path and shape instability, there is a need to describe the path and shape transition in high viscous massecuite equivalent fluids for this current research.

2. Rheological characterisation

Rheology is the study of the science of deformation and flow of matter. One of the key tasks of rheology is to establish the relationships between characteristics such as shear stress and strain and its derivatives (Bhattacharya, 1997). Polymer solutions often demonstrate non-Newtonian flow behaviour. Such fluids commonly have a viscosity that depends on the shear rate and display elastic effects like normal stresses that greatly affect their response to deformation. Usually, when polymers are under low shear, the viscosity is high. As the shear rate increases, the viscosity decreases. Generally the viscosity increases again as the shear force reduced. This behaviour is called shear thinning.

The natures of Polyacrylamide (PAM), Xanthan gum (XG) and crystal suspensions were usually known to demonstrate shear thinning behaviour, as the viscosity of these materials

decreases with higher applied shear rates (Hassan *et al.,* 2010b). The "Power Law" model was generally used to describe the non-Newtonian behaviour of these materials.

The rheological properties for three (0.025%, 0.05% and 0.1%) concentrations of the various polymer solutions and crystal suspensions were measured using an ARES Rheometer with bob and cup geometry. For rheological test, the diameters used for bob and cup were 25 mm and 27 mm respectively producing a gap of 1 mm between them. The samples were poured into the cup, and then lowered the bob until the upper surface bob was 1 to 2 mm below the surface of the sample. It is noted that the upper surface of the bob must be between zero and five mm below the upper surface of the cup. The rheological properties of these solutions are summarised in Table 1. The range of shear rates used to determine fluid rheology was 1-100 s^{-1} (Hassan *et al.,* 2007a, 2007b; Hassan *et al.,* 2008a, 2008b; Hassan *et al.,* 2010b; Hassan, 2011).

Fluid Type	Viscosity, $Pa.s$ at 1 s^{-1} (shear rate)	Viscosity, $Pa.s$ at 100 s^{-1} (shear rate)	Fluid consistency, K, $Pa.s^n$	Power law index, n
Polyacrylamide, 0.025% (by weight)	0.004	0.003	0.005	0.85
Polyacrylamide, 0.05% (by weight)	0.035	0.007	0.035	0.62
Polyacrylamide, 0.1% (by weight)	0.10	0.013	0.09	0.60
Xanthan Gum, 0.025 % (by weight)	0.008	0.003	0.007	0.77
Xanthan Gum, 0.05% (by weight)	0.039	0.006	0.039	0.71
Xanthan Gum, 0.1% (by weight)	0.11	0.012	0.10	0.57
Xanthan gum crystal suspension: 0.05% xanthan gum + 1% polystyrene (by weight)	0.11	0.006	0.11	0.63

Table 1. Rheological properties of non-Newtonian solution

The fluid consistency index (K) and power law index (n) for all solutions were determined from the response curve of shear rate against shear stress. The storage modulus (G'), the loss modulus (G'') of polymer solutions and crystal suspension solutions were tested (Hassan, 2011). The storage modulus (G′) and the loss modulus (G′′) of polymeric solutions and crystal suspensions were also investigated. G′ measures the energy stored and recovered per cycle, when various fluids are compared at the same strain amplitude. It is a measure of the elasticity of the system. G′′ measures the energy dissipated or lost for each cycle of sinusoidal deformation, when fluids are compared at the same strain amplitude. It is the measured viscous response of the system.

A comprehensive explanation of fluid flow curves for different polymeric solutions and selection of crystal suspended non-Newtonian fluid are presented in later sections. The values of n, K, G', G'' and the response curves (shear stress against shear rate and viscosity

against shear rate) of non-Newtonian fluids were compared with the literature data of the massecuite fluid for determining the massecuite equivalent non-Newtonian crystal suspension fluid (Hassan, 2011)

2.1. Viscosity of polymer solutions

The viscosities as a function of shear rate for 0.025%, 0.05% and 0.1% concentrations of PAM solutions tested are presented in Figure 4. Examination of Figure 4 indicates that these three concentrations of PAM solutions exhibit non-Newtonian shear-thinning flow behaviour over the shear rates tested. It shows that the viscosity of these polymer solutions increases with the increase in PAM concentration with the 0.1% concentration has higher viscosity than the other two concentrations.

Viscosities as a function of shear rate for 0.025%, 0.05% and 0.1% concentrations of XG solutions are plotted in Figure 5. The same phenomenon as seen for PAM was observed for the three concentrations of XG solutions. The viscosity in XG solutions for all concentrations was found to be relatively higher in comparison with the PAM solutions, and its shear thinning effect (slope) was more pronounced for the entire range presented.

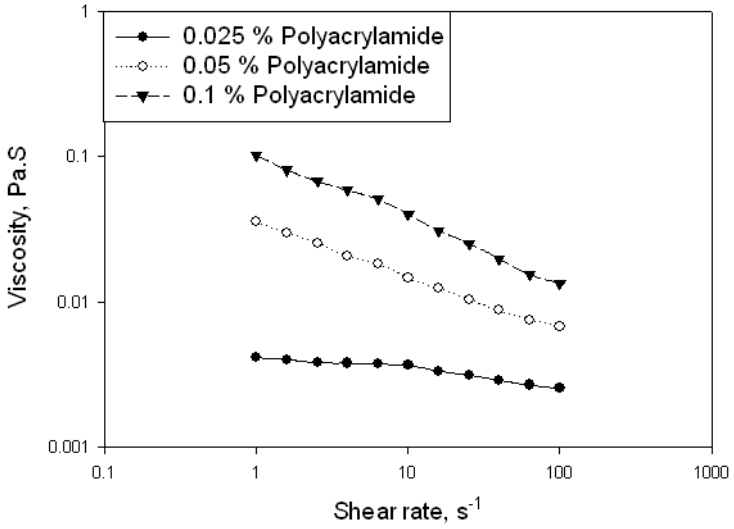

Figure 4. Viscosity versus shear rate of different concentrations of polyacrylamide solutions

2.2. Power law and fluid consistency index

Figure 6 presents n and K values in terms of fluid concentrations for different liquids. The figure shows that the K value for PAM solution concentrations was observed to be less than that in the corresponding XG solution concentrations. XG showed a higher viscous property (K) in comparison with PAM solution.

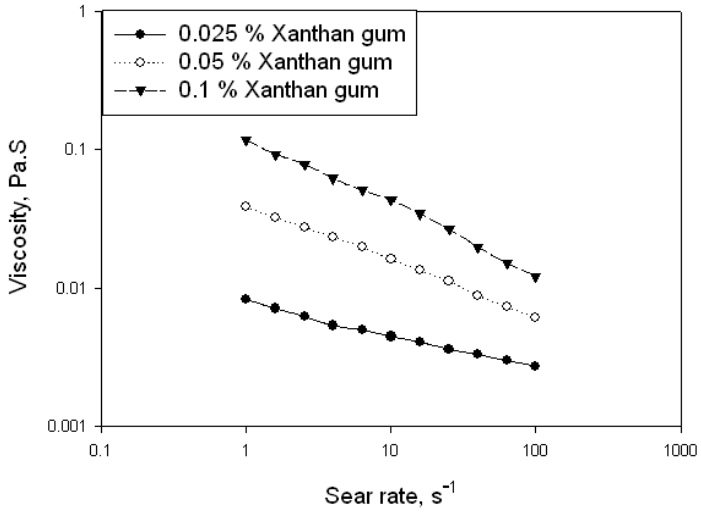

Figure 5. Viscosity versus shear rate of different concentrations of xanthan gum solutions

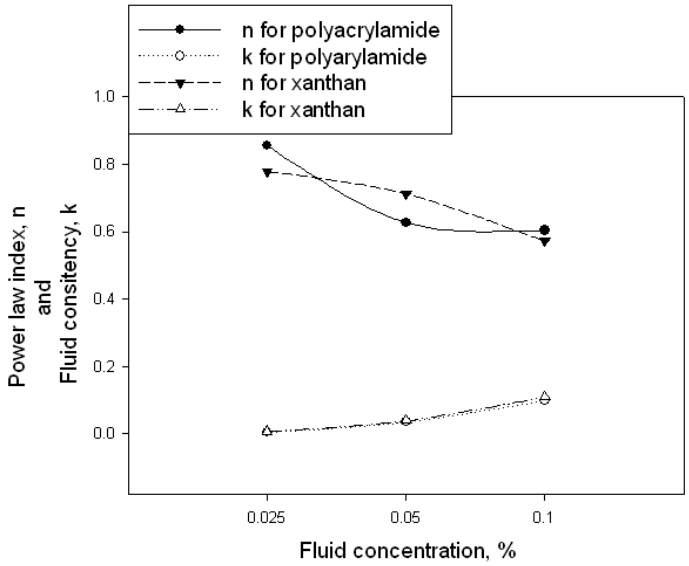

Figure 6. Power law index (n) and fluid consistency index (K) as a function of fluid concentration

It is also seen that the n generally decreases with the increase in liquid concentration for the three fluids. The value of n was observed lowest for 0.1% concentration of PAM and was highest for 0.025% PAM solution. On the other hand, 0.05% XG has the highest n value in comparison with the other liquid corresponding to the same concentration.

After analysing all the fluids used in this work, it is clear that the value of K for XG and PAM solutions increases with increase in concentration. This is expected since K is a direct function of the viscosity whilst the value of n which is less than unity, signifies the degree of shear thinning effect.

Two concentrations of 0.025%, and 0.05% of PAM and XG were used for bubble rise experiments as the higher concentrations of these fluids are not visually clear.

2.3. Viscoelastic property of polymer solutions

Storage modulus (G′) or elastic response and loss modulus (G″) or viscous response for 0.1% concentration of PAM solutions as a function of frequency are shown in Figure 7. The relevance and the definition of G′ and G″ in relation to the current study are discussed in Section 2.

PAM solution shows both viscous and elastic responses, with the elastic effects being more dominant than the viscous effects. This phenomenon can be observed in Figure 7 where PAM solutions with 0.1% concentrations showed more elastic response at higher shear rates. G′ and G″ of 0.025% and 0.05% concentrations of PAM solutions are not shown since they showed a similar phenomena to that of 0.1% concentration.

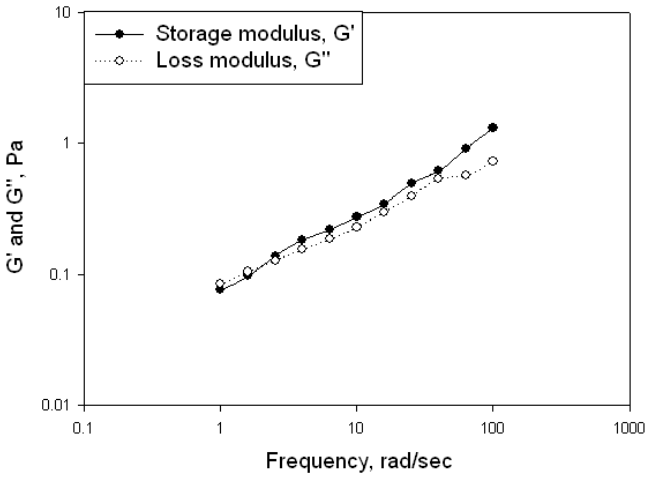

Figure 7. Storage modulus (G′) and loss modulus (G″) versus frequency for 0.1% polyacrylamide

G′ and G″ for three concentrations of xanthan gum solutions as a function of frequency are illustrated in Figures 8, 9 and10 respectively.

XG solutions have shown both viscous and elastic responses, with viscous effects more dominant than elastic effects at the range of lower frequency. It is seen from Figure 8 that XG solution with 0.025% concentration exhibited more viscous response in comparison with the elastic response. However, it exhibits similar elastic and viscous responses at the higher frequency range.

In Figure 9, the viscous response was more pronounced than the elastic response at the lower and higher frequency range. On the other hand, examination of Figure 10 indicates that the elastic response was more pronounced than the viscous response at the higher frequency range.

Therefore it can be concluded that the viscous effects of the XG solutions were more pronounced than elastic effects, and this behaviour was similar to that observed with high grade massecuites.

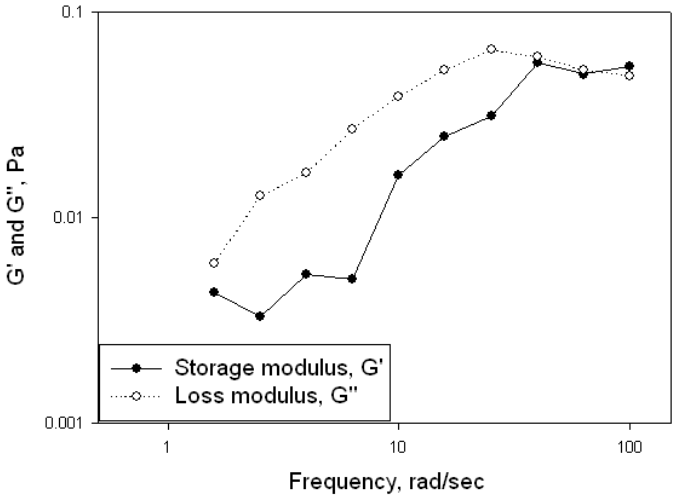

Figure 8. Storage modulus (G′) and loss modulus (G″) versus frequency for 0.025% xanthan gum

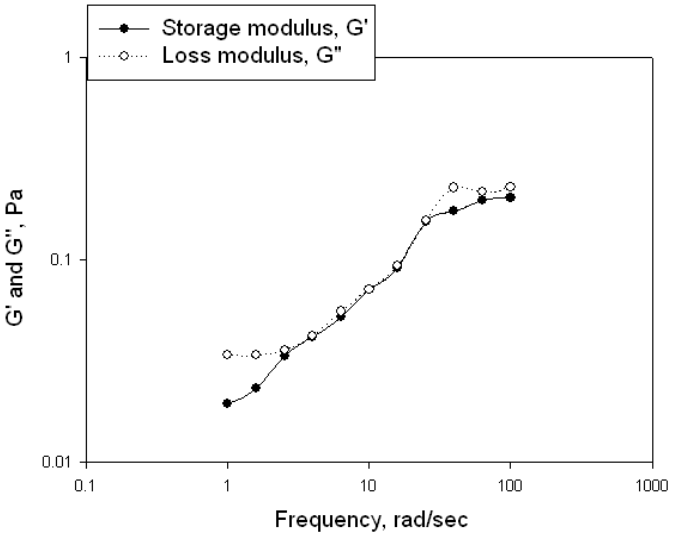

Figure 9. Storage modulus (G′) and loss modulus (G″) versus frequency for 0.05% xanthan gum

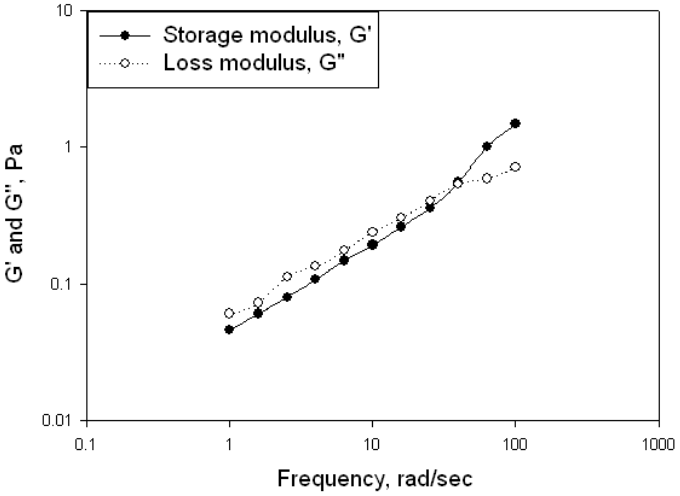

Figure 10. Storage modulus (G′) and loss modulus (G″) versus frequency for 0.025% xanthan gum

2.4. Selection of crystal suspension

The uses of bubbles are very significant in vacuum pan operation in the sugar industry. Vacuum pans (large cylindrical vessels with vertical heating surfaces) are used to process the massecuite - a fluid made from sugar crystals and mother sugar syrup (molasses) (Hassan et al., 2010a, 2010b; Hassan, 2011). Usually, massecuites show non-Newtonian shear thinning behaviour at lower shear rates; that is the viscosity is highest at low shear rates and decreases with increasing shear rates (Ness, 1983; Broadfoot and Miller, 1990). But massecuites are not optically clear and, in non-industrial environments, massecuites endure problems due to degradation during storage and changing rheological properties under different temperature conditions.

The properties of massecuites depend on concentration of sugar crystals and their purity. Generally, massecuites are described as exhibiting shear thinning behaviour (Broadfoot *et al*., 1998; Broadfoot and Miller, 1990; Adkins, 1951). It has been shown that the power law model does give a good fit to experimental data (Ness, 1983; Broadfoot and Miller, 1990; Bojcic *et al*., 1997; Broadfoot, 1998). Temperature has also been shown to affect viscosity through changing the values of K and n (Broadfoot *et al*., 1998; Ness, 1983; Broadfoot and Miller, 1990; Awang and White, 1976). When determining the effect of viscosity on bubble rise in three phase materials such as massecuites (solid-liquid-gas; sugar crystal – molasses – vapour), the characteristics of the bubble rise are dependent on the liquid viscosity (molasses) rather than the mixture viscosity (molasses plus crystals). Literature also suggests that the viscosity of molasses is less than the mixture viscosity of massecuites (Rackemann, 2005; Ness, 1983; Broadfoot and Miller, 1990; Adkins, 1951; Nezhad, 2008; Hassan, 2011).

As mentioned earlier, massecuites are not optically clear. Therefore a fluid needs to be prepared to replicate the massecuite with an equivalent non-Newtonian fluid for studying

the bubble rise characteristics which is optically clear and has similar rheological properties to that of the massecuite.

Figure 11 shows the viscosity – shear rate flow curve of a high grade massecuite (Type A). Also shown in Figure 11 are the shear rate flow curves for 0.05% of XG with different percentages of crystal.

Observation from Figure 11 indicates that different crystal suspended XG solutions exhibit non-Newtonian shear-thinning flow behaviour. The viscosity of these crystal suspensions increases with the increase in crystal concentration, with the shear thinning effect (slope) more pronounced over the range of shear rates presented. The XG solution with 25% crystal concentration has the highest viscosity and the lowest power law index in comparison with the other concentrations used in this study. However, the 5%, 10% and 25% crystal suspensions were not optically clear enough to visually observe the bubble rise. After analysing all the solutions in Figure 11, it is seen that the flow curve of XG solution (0.05% XG by weight) with 1% crystal content exhibits similar rheological characteristics to that of high grade massecuite for the range of shear rate presented; also it was optically clear. In other words, the viscosity of the crystal suspension is not exactly the same, but it shows close similarity with power law index, fluid consistency and shear thinning flow behaviour to that of high grade massecuite and molasses.

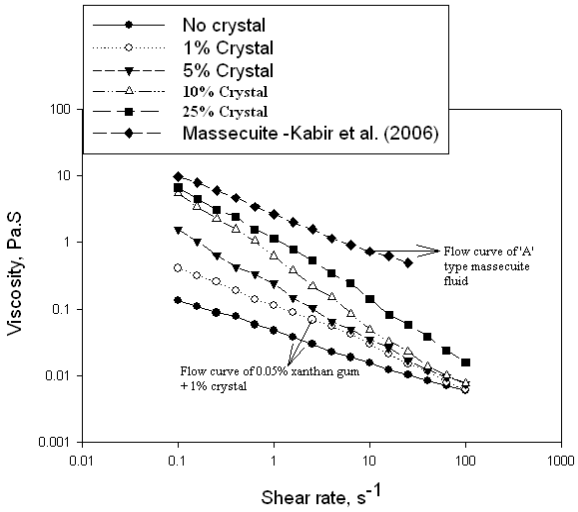

Figure 11. Viscosity versus shear rate of 0.05% xanthan gum solutions with different percentages of crystal content and massecuite of 40% crystal content at 65 °C (Hassan *et al.,* 2010b, Kabir *et al.,* 2006)

However, XG crystal suspension showed both viscous and elastic responses with the viscous effects more dominant than the elastic effects. This phenomenon is shown in Figure 12 where XG crystal suspension displays more viscous response at very low and very high shear rates and this is also similar to that high grade of massecuite.

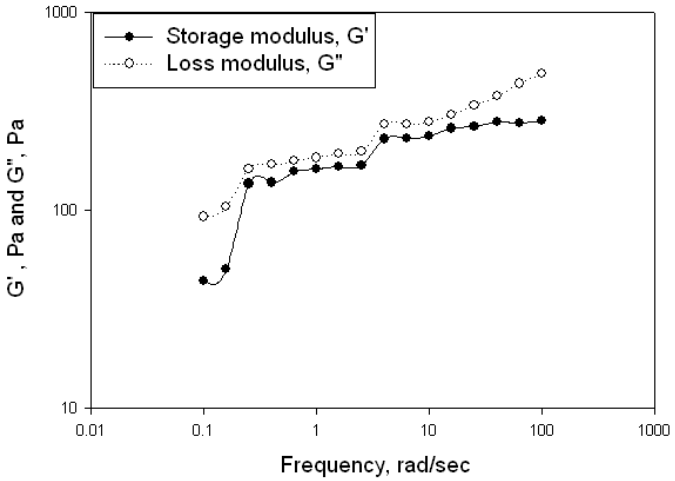

Figure 12. Storage modulus (G′) and loss modulus (G″) versus frequency for 0.05% xanthan gum + 1% crystal (Hassan *et al.,* 2010b)

3. Experimental setup

The experimental set-up consisted of transparent cylinders to hold fluids and bubble insertion mechanism and video camera lifting apparatus. A schematic of the experimental set-up is shown in Figure 13.

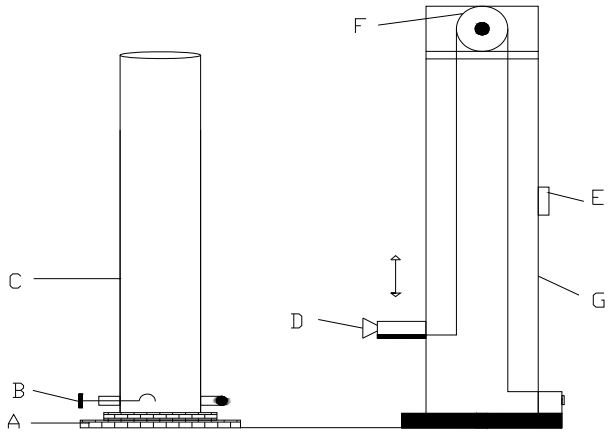

Figure 13. Schematic diagram of experimental apparatus

where A = Sturdy base; B = Rotating spoon; C = Cylindrical test rig (125mm or 400 mm diameter), D = Video camera; E = Variable speed motor; F = Pulley; and G = Camera lifting apparatus.

Two-test rigs were designed and fabricated for investigating the bubble rise characteristics in Newtonian and non-Newtonian fluids. Rig 'A' consists of a polycarbonate tube approximately 1.8 m in height and 125 mm in diameter as shown in Figure 14.

The polycarbonate material was chosen for optical clarity to enable precise visual observation. Rig A has a sturdy base and is capped with suitable connections to allow the rig to operate under partial vacuum conditions. It also contains two holes near the base. One is to facilitate the removal of the fluid contained in it and the other is to insert air bubbles into the test rig. The insertion mechanism, shown in Figure 15, consists of a ladle or spoon with a small pipe running down the centre that has a capability to control the injection of air. The air was injected through this pipe into the upside-down ladle using a syringe. The cup was then twisted to allow the bubble to rise.

Rig B (shown in Figure 14) consists of an acrylic tube of 400 mm in diameter and 2.0 m in height with the same connections for bubble insertion and fluid draining in test Rig A. Rig B was employed to examine the larger sizes of bubble to eliminate the wall effect.

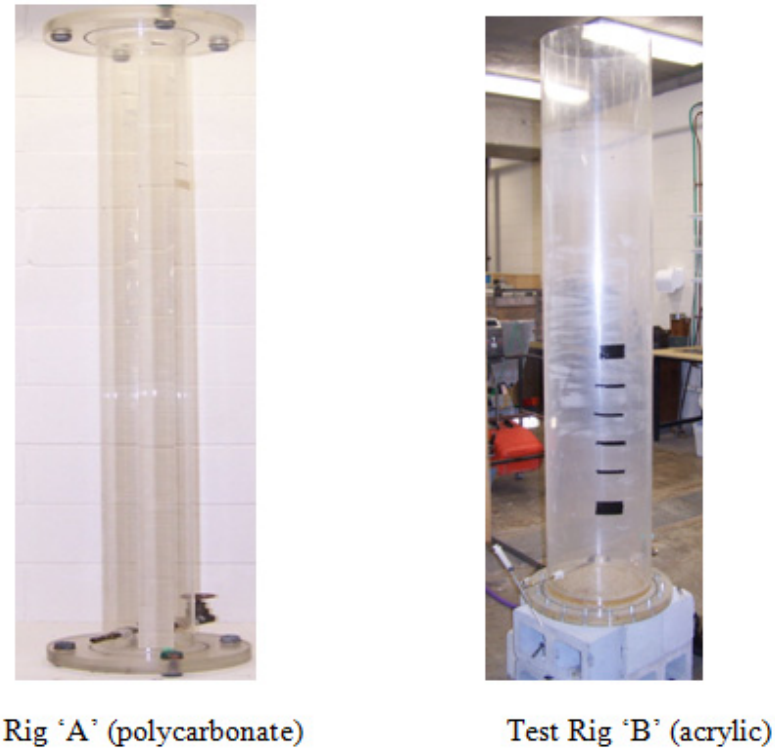

Figure 14. Photographs of test rig A and B

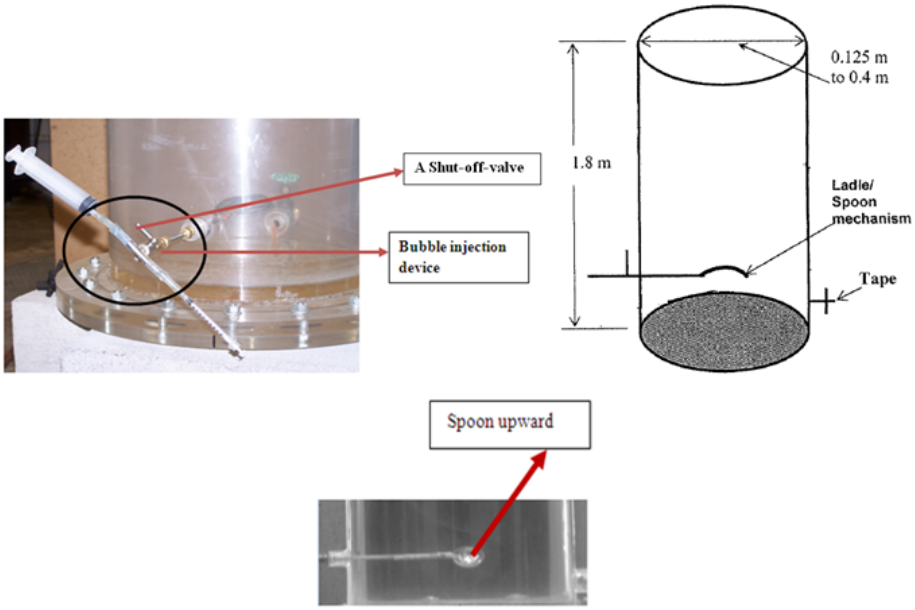

Figure 15. Bubble insertion mechanisms

4. Experimental procedure

4.1. Determination of bubble shape

The still images were taken in order to determine the bubble shape. A charge-coupled device (CCD) digital camera was used to capture the 2D bubble shapes (height and width) using the commercial software SigmaScan Pro 5.0 and Adobe Photoshop: DV Studio version 3.1E-SE. These images were analysed in order to determine the size and the aspect ratio of each bubble. Only a complete good quality recorded images was taken into account. Blurred images were ignored as the accuracy of the bubble size determination depends on the quality of the picture.

4.2. Determination of bubble diameter

Bubble equivalent diameter was measured from the still images which were obtained from the video clips. The still images were analysed using commercial software "SigmaScan Pro 5.0" and the bubble height (d_h) and the bubble width (d_w) were measured in pixels. The pixel measurements were converted to millimetres based on calibration data for the camera. The bubble equivalent diameter d_{eq} was calculated (Lima-Ochoterena and Zenit, 2003) as:

$$d_{eq} = \left(d_h \times {d_w}^2\right)^{\frac{1}{3}} \tag{14}$$

For this measurement it was assumed that the bubble is axi-symmetric with respect to its minor axis direction as shown in Figure 16.

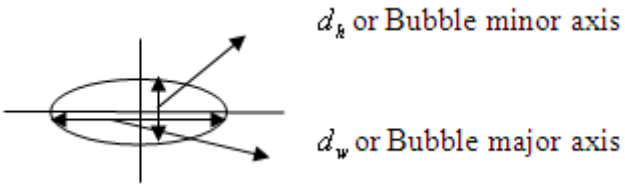

Figure 16. Bubble major and minor axes

This equivalent diameter was used for the calculation for bubble eccentricity, bubble deformation parameter, Reynolds number and bubble drag co-efficient.

4.3. Determination of bubble trajectory

Bubble trajectory was computed from the still frames obtained from the video image. The still frame was opened in "SigmaScan Pro" commercial software, which was capable of showing pixel location on an image.

The pixel coordinates (X and Y) of the bubble's centre were noted and recorded into the spreadsheet. The X and Y coordinates correspond to the distance from the left and top edges respectively. The pixel line running through the centre of the bubble release point was known. The deviation of the bubble centre from the release point was computed by subtracting the X-location of the bubble centre from the X-location of the bubble release point.

A linear equation was developed for the determination of the rigs X pixel coordinate for a given Y coordinate. This was used in association with the Y of the bubble's centre for the correction of any changes which might occur based on the bubble's location (e.g. if the bubble is at the top of the image, the tube's centre is slightly to the left than if the bubbles were at the lower portion of the image).

Still frames from the digital video camera captures images where the camera can see two of the markers. The number of pixels that separates these two markers was used in association with their real separation in millimetres, which was 100 mm. Consequently, a conversion factor was made to change distances in pixels to distance in millimetres. Using this conversion factor, the deviation of the bubble from the tube's centre was converted into millimetres.

5. Results and discussions

The results of the behaviour of bubbles' motions and their transition, and shapes encountered and their oscillations are reported in the next section. Different bubble volumes (0.1 mL, 2.0 mL, 5.0 mL and 10.0 mL) were used at 1.0 m height of the liquid column for the calculation of bubbles' trajectories and shapes.

5.1. Bubble trajectory in Newtonian and non-Newtonian Fluids

The trajectory experimental results for 5.76 mm diameter bubbles are shown in Figure 17 for different liquids when measured over a height of 1 m from the point of air injection. Figure 17 shows the deviation of the bubble from its release point as it rises through the liquids. The general trend is for the bubble to remain close to the line of the release centre when the bubble is released and, as it rises through the liquids, it spreads out progressively as the height increases.

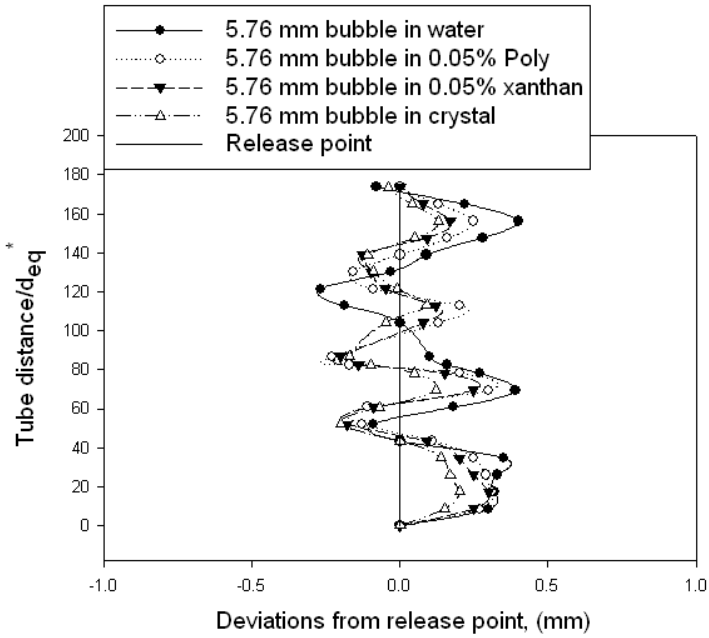

Figure 17. Experimental rise trajectories for 5.76 mm diameter (0.01 mL) bubbles in different liquids

It is seen from the experiments that the smaller bubble of 5.76 mm diameter deviated horizontally more in water than in the other three liquids, and the bubble shows a zigzag motion in all liquids. But the zigzag motion was produced more in water compared to other two liquids. The horizontal movement in 0.05% PAM and XG polymer solutions was observed to be less than that in water, and was the least in crystal suspension. This phenomenon agrees well with the experimental findings of Saffman (1956) and was reported by Hassan *et al.* (2008a; 2008b; 2008c; 2010a). The lesser horizontal deviations observed in the case of polymers and crystal suspensions are due to the higher effective viscosity of these liquids than that of water and a smaller Re of a given bubble. Hence, the vorticity produced at the bubble surface by the shear-free condition is also smaller, since this surface vorticity is an increasing function of Re until it becomes independent of Re for a large enough value. This smaller surface vorticity produces a less unstable wake resulting in smaller horizontal motions.

Smaller bubbles less than 2 mm in diameter rise in water in a straight or rectilinear path (Clift *et al.*, 1978; Duineveld, 1995), but the linear trajectory in all liquids was not observed as the bubble equivalent diameter of this study was equal to or more than 5.76 mm. However, the path of a rising bubble is not always straight. The shape of the bubble was found to be stable for very low *We* , and it turned into an oscillatory or unstable shape for larger *We* . At low Re and *We* for smaller bubbles, the rising bubble showed a zigzag trajectory. The zigzag motion is due to an interaction between the instability of the straight trajectory and that of the wake. The periodic oscillation of the wake is somewhat less in the crystal suspension due to the increase in viscosity. When a bubble rises in liquids, the bubble experiences both a lateral force and a torque along its path and two counter-rotating trailing vortices appear behind the bubble; hence its path, changes from a straight trajectory to a zigzag trajectory (Mougin and Magnaudet, 2006).

The trajectory experimental results for 15.63 mm diameter bubbles are illustrated in Figure 18.

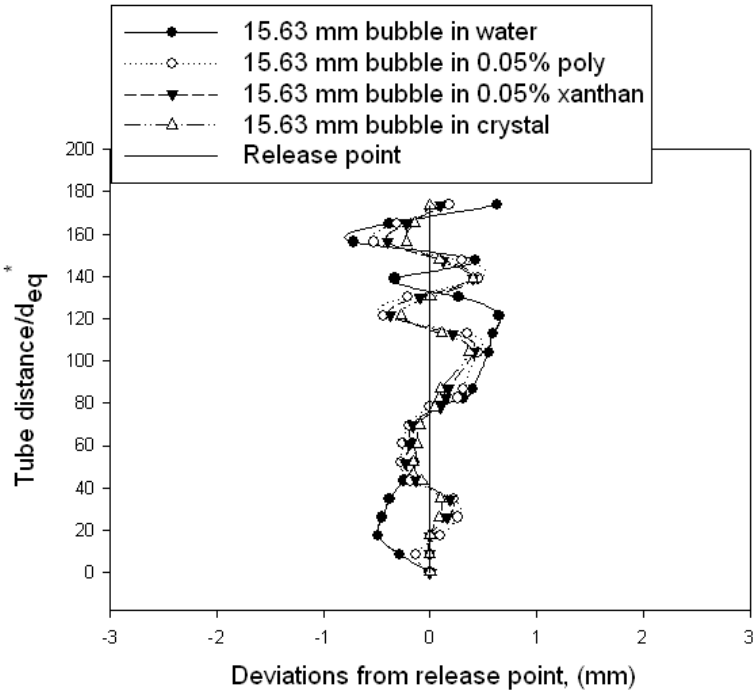

Figure 18. Experimental rise trajectories for 15.63 mm diameter (2 mL) bubbles in different liquids

With increasing bubble size, the bubble shape changes from spherical to ellipsoidal, the bubble surface oscillations transform from a simple oscillation to higher order forms, and the trajectory changes from a simple zigzag to more spiral trajectories. The bubble of 15.63 mm in water initially deviated horizontally, then followed a spiral motion and finally

attained a zigzag path. However, the 15.63 mm bubble initially followed a straight path, then it followed only a zigzag motion in polymer solutions and crystal suspension until it finished its journey.

The trajectory experimental results for 21.21 mm bubbles are plotted in Figure 19. As seen from the experiments, the 21.21 mm bubbles initially choose the zigzag motion, and finally switch to a spiral path for all liquids. The transition from zigzag to spiral motion was also observed by Aybers and Tapucu (1969) as the bubble size increases. The transition from zigzag to spiral is also consistent with observations found in the literature (Saffman, 1956). For bubbles of size 15.63 mm and 21.21 mm, path instability occurs as the bubble size increases.

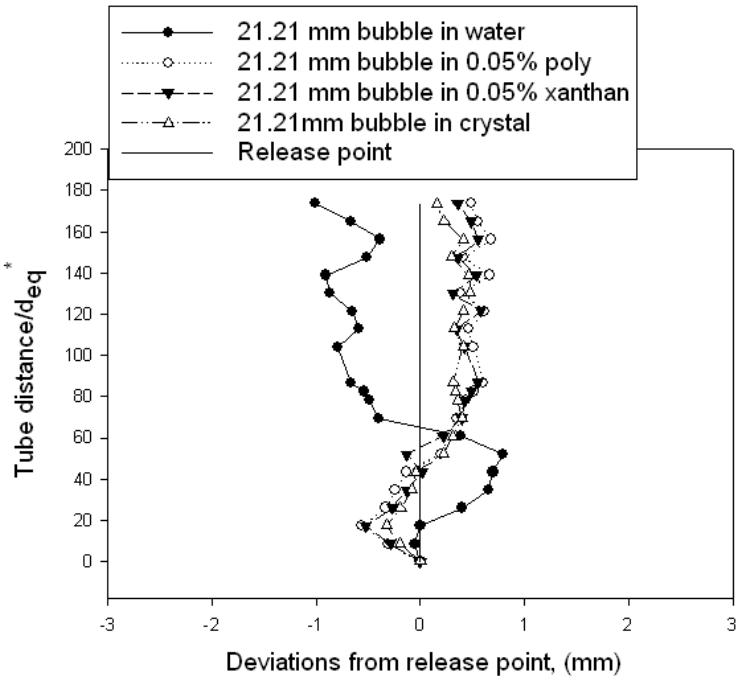

Figure 19. Experimental rise trajectories for 21.21 mm diameter (5 mL) bubbles in different liquids

No zigzag motion was observed for the larger bubble of 26.84 mm as seen in Figure 20 for water. The trajectory of these bubbles totally changed into a spiral motion. These bubbles initially choose a straight path and finally, they switch to a spiral path. It is seen from Figure 20 that the 26.84 mm bubble shows more spiral motion than the 21.21 mm bubble.

The crystal suspended xanthan gum produced more spiral motion in comparison with water and polymer solutions. The larger bubbles however experience more resistance on top and deform as their size increases. Furthermore, it can be confirmed that path instability was seen for ellipsoidal bubbles of sizes 2 mL and 5 mL only, and not for the 10 mL bubble.

This is consistent with the findings by other researchers (Haberman and Morton, 1954; Aybers and Tapucu, 1969; Wegener and Parlange, 1973; Shew *et al.*, 2006; Hassan *et. al.*, 2010a).

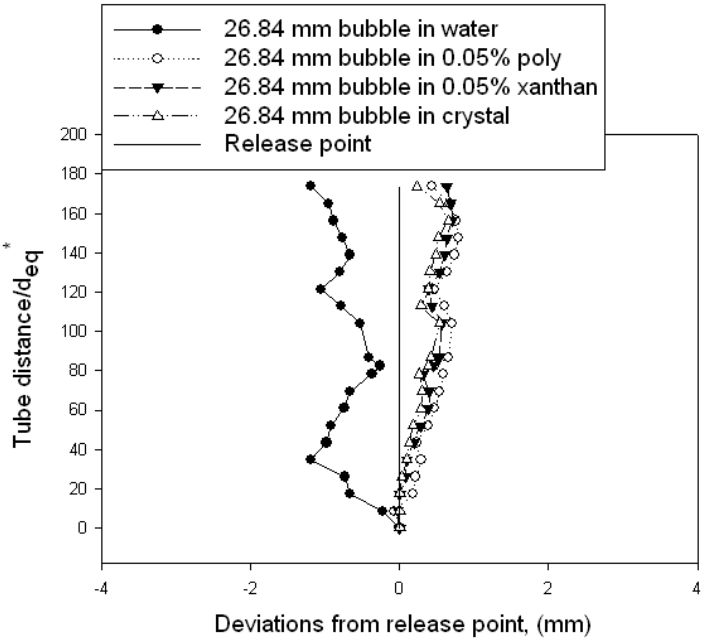

Figure 20. Experimental rise trajectories for 26.84 mm diameter (10 mL) bubbles in different liquids

5.2. Influences of Re, We and Mo on bubble trajectory

The observed Weber number as a function of bubble equivalent diameter in water, polymer solutions and crystal suspension is plotted in Figure 21. It is observed that We increases with increase in bubble equivalent diameter. As seen in Figure 21, the horizontal lines indicate the critical Weber number (We_{cr}) that must be exceeded for path transition to occur. In this study, the values of We_{cr} were measured for water, $We_{cr} \approx 3$; 0.05% xanthan gum, $We_{cr} = 6.31$, 0.05% polyacrylamide $We_{cr} = 6.13$ and crystal suspension, $We_{cr} = 7.9$ (Hassan, 2011). The equation 11 was used to calculate the We_{cr} .It is seen from Figure 21 that the measured We_{cr} in water shows consistent results with published literature (Hartunian and Shears, 1957; Aybers and Tapucu, 1969; Duineveld, 1994; 1995). Observations from Figure 21 also indicate that the We_{cr} at which the transition to oscillatory path behaviour commences is the least for water and the most for crystal suspension. Therefore, the path transition initiation of bubble rise in crystal suspension is less rapid than in water. The reason for this is that the Mo is different for these four liquids and is much higher for the

crystal suspension than for water. As a result the observed change suggests that the *We* is not entirely responsible to characterise the bubble path transition. Hence, for a given *We*, the deformation is much less in crystal suspension than in water, and the vorticity produced is also less in crystal than that in water.

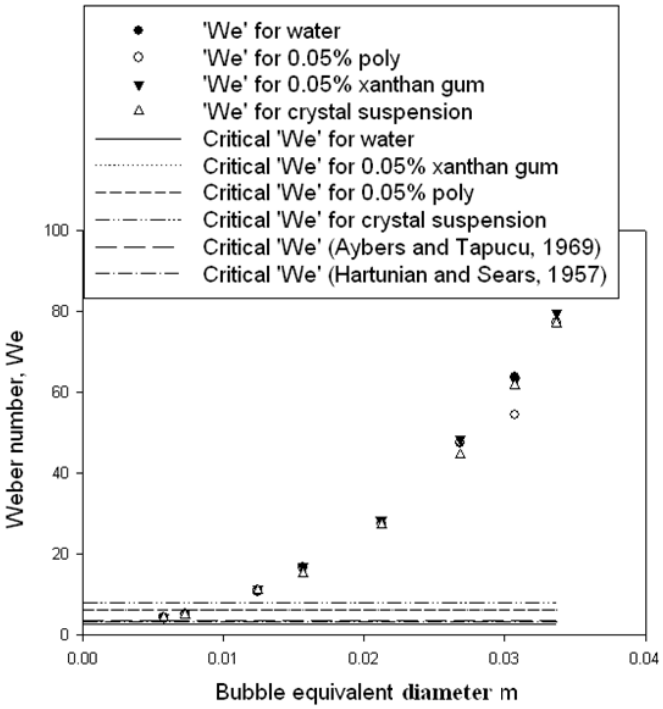

Figure 21. Weber number as a function of the bubble equivalent diameter (Hassan *et al.*, 2010a)

The effects of Re and *We* values on bubble trajectory in crystal suspension are discussed below for three regions. The characteristics of bubble rise corresponding to Re and *We* are also summarised in Table 2. At low Re and *We* for smaller bubbles (5.76 mm), the rising bubble shows a zigzag trajectory. For the intermediate region, the bubble of size 15.63 mm shows both zigzag and spiral trajectories. It is noted that path instability occurred in this region due to increase in bubble size and unstable wake structure. At moderately high *We* and Re, the bubbles deform and change from spherical to ellipsoidal and experience more surface tension and inertia force which induces both zigzag and spiral trajectories. At very high Re and *We*, larger bubbles (> 21.21 mm) produce a spiral motion in all liquids as the effect of wake shedding influences the bubble to induce a spiralling rising motion.

Bubble size, mm	Re	*We*	We_{cr}	Bubble shape	Region of Re and *We* values	Zigzag motion	Spiral motion
5.76	45.78	4.33	7.9	Nearly Spherical	Low	√	×
15.63	102.06	15.10		Ellipsoidal	Intermediate	√	√
21.21	150.37	27.30		Ellipsoidal or Ellipsoidal cap	Moderately high	√	√
26.84	207.91	44.60		Ellipsoidal or Spherical cap	Very high	×	√

Table 2. The characteristics of bubbles corresponding to Re *and We* for crystal suspension (Hassan, et al., 2010a; Hassan, 2011)

5.3. Bubble shapes encountered in different liquids

5.3.1. Bubble shapes in water

Grace *et al.,* (1976) constructed the so called "shape maps" as shown in Figure 3 in earlier section. It has been proven to be a quite useful qualitative method for measuring the shapes of bubbles for Newtonian liquids, based on dimensionless quantities such as Re and *Eo* , with *Mo* being a parameter with specific values for specific liquids. The shapes are predicted in comparison with the "shape maps" on the basis of visual observations. In this study, bubble shapes predicted in water at three different heights are presented in Table 3, and *Eo* against Re with the *Mo* parameter for water is shown in Figure 22 As seen from Figure 22, *Eo* increases with increase in Re with low *Mo* liquids. Furthermore, Re with the variation of bubble equivalent diameter is shown in Figure 23. As seen from Figure 23, the bubble equivalent diameter also increases with increase in Re . It is also observed that *Eo* increases with increase in bubble equivalent diameter. Therefore it can be concluded that Re and *Eo* have a greater influence on bubble shapes.

Observations from Table 3 and Figure 23 indicate that nearly spherical shapes were observed at small values of *Eo* and *Re* at three different heights. Ellipsoidal bubbles were encountered at moderate Re and *Eo.* Usually, ellipsoidal bubbles are termed as oblateness with a convex interface around the surface (Clift *et al.,* 1978). The transition from spherical to ellipsoidal is due to the surface tension and inertia effects on bubble surface. Finally, the ellipsoidal cap or spherical cap shape occurred only at very high Re and high *Eo*. In addition, a wobbling shape was also found at 0.5 m height for 5.0 mL bubble in high Re region. Wobbling shapes were mainly found at sufficiently high Re and *Eo* . This shape is

mainly occurred due to the un-symmetric vorticity created in the bubble wake and the instability of bubble interface. In this region the bubble shows oscillating behaviour as the bubble velocity increases with increase in bubble size. The wobbling bubbles were also noticed by Clift *et al.* (1978) in high *Re* region of the ellipsoidal regime of Grace's (1976) shape maps.

a. Different bubble shapes at 0.1 m height			
0.1 mL (5.76 mm)	2 mL (15.63 mm)	5 mL (21.21 mm)	10 mL (26.84 mm)
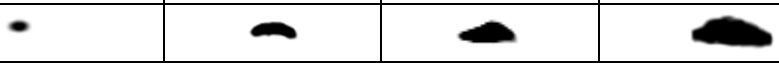			
b. Different bubble shapes at 0.5 m height			
0.1 mL	2 mL	5 mL	10 mL
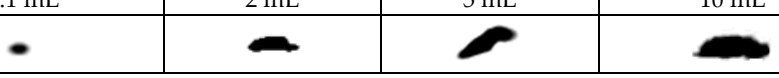			
c. Different bubble shapes at 1 m height			
0.1 mL	2 mL	5 mL	10 mL
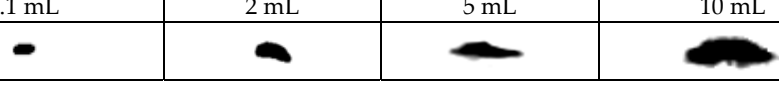			

Table 3. Bubble shapes observed in water at three different heights

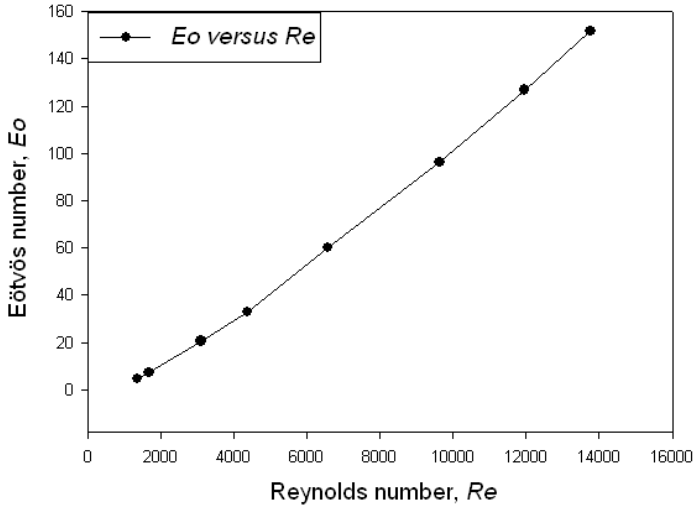

Figure 22. *Eo* versus *Re* with Mo as parameter ($Mo = 2.502 \times 10^{-11}$) for water

At higher *Eo* and Re , the bubbles usually exhibit noticeable deformation, and therefore they become ellipsoidal and consequently they have a spherical cap shape. These shapes encountered in water are consistent with the published literature of Grace (1976), Clift *et al.*, (1978) and Bhaga and Weber (1981).

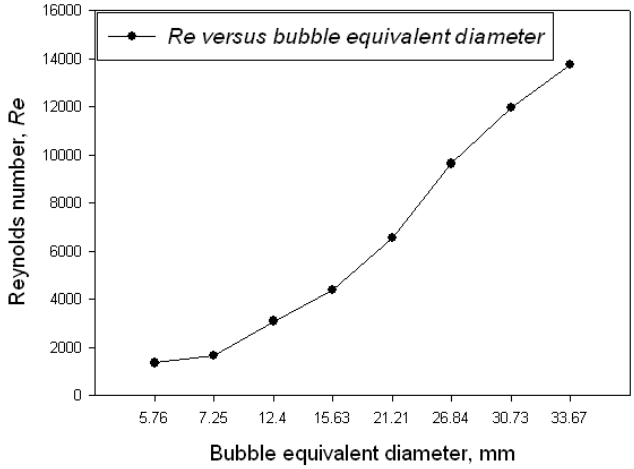

Figure 23. *Re* versus bubble equivalent diameter

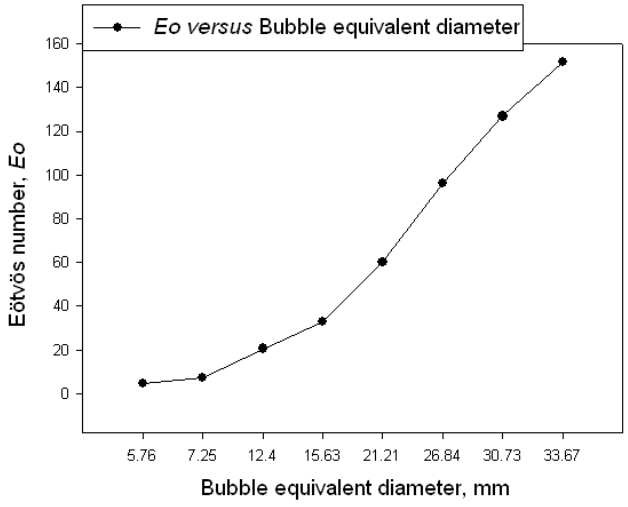

Figure 24. *Eo* versus bubble equivalent diameter

5.3.2. Bubble shapes in polymeric solutions

Tables 4 and 5 summarise the different bubbles shapes observed in 0.05% XG and 0.05% PAM. As seen from Tables 4 and 5, different bubble shapes were encountered apart from the spherical, ellipsoidal and spherical-cap. Usually, the bubble shapes are greatly dependent on *Re, Eo* and the aspect ratio or eccentricity of bubble, E . The bubble shapes in terms of bubble eccentricity (which is defined as the ratio of maximum bubble width to the maximum bubble height) are also dependent on rheological properties of the liquids. The literature

suggests that prolate shaped (E < 1) and oblate shaped bubbles (E > 1) are usually observed in non-Newtonian viscoelastic liquids (Acharya, 1977). The bubble shapes observed in this study are mainly oblate shaped as the eccentricity was found to be greater than 1.

The bubbles usually deformed as their size increased and the rate of deformations were more pronounced at higher values of Re, Eo and E. As evidenced from Figures 25 and 26, Re increases with the increase of Eo and E, meaning that for higher Re and Eo bubbles become more flat due to the higher bubble velocity.

At lower values of Re, Eo and E, bubbles shapes were observed to be nearly spherical in 0.05% XG and 0.05% PAM. With a further increase in Re, Eo and E, the bubbles become flat and appear to be an oblate shape for both liquids. As seen from Table 5, the bubble appears to have a skirted shape at 1.0 m height for the 2.0 mL bubble in PAM solution. The skirt region near the rear of the bubble becomes thin, and with further increase of Re, Eo and E, the skirt would turn out to be thinner and unstable, as is evidenced in Table 5 for the 5.0 mL bubble size corresponding to the same liquid. For larger bubble size (10.0 mL), it turns into an ellipsoidal cap shape at very high Re, Eo and E. The ellipsoidal cap shaped bubble was also noticed in 0.05% XG solutions at 1.0 m height for the 10.0 ml bubble. Besides their usual shapes, wobbling bubbles were also encountered in 0.05% XG solution for 2.0 mL and 5.0 mL of bubbles. This is due to the bottom part of the bubble experiences deformations resulting from the unstable and non symmetrical bubble wake. In particular, the irregular pairs of secondary vortices are also created in the wake as a result of the separation of the boundary layer from different sides of the bubble surface. These observed shapes are consistent with the published literature (Clift *et al.,* 1978; Bhaga and Weber, 1981).

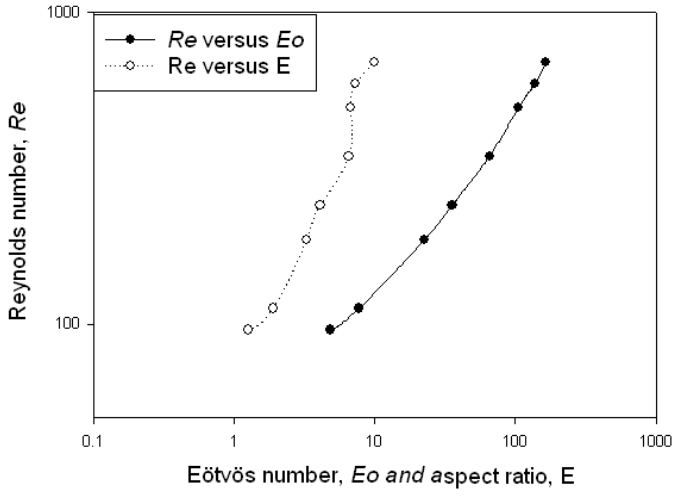

Figure 25. *Re* versus *Eo* and E for 0.05% xanthan gum

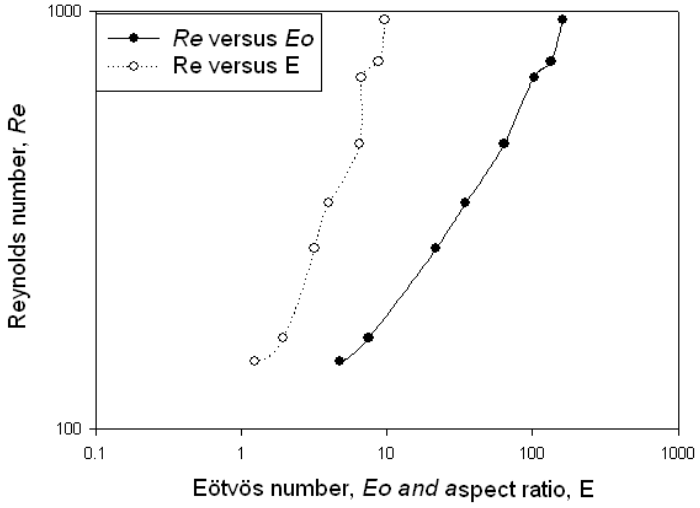

Figure 26. *Re* versus *Eo* and E for 0.05% polyacrylamide

a. Different bubble shapes at 0.1 m height			
0.1 mL	2 mL	5 mL	10 mL
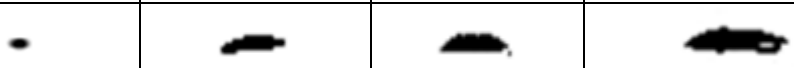			
b. Different bubble shapes at 0.5 m height			
0.1 mL	2 mL	5 mL	10 mL
			
c. Different bubble shapes at 1 m height			
0.1 mL	2 mL	5 mL	10 mL
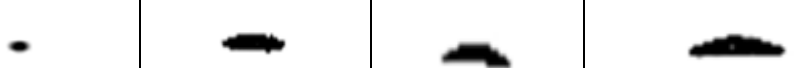			

Table 4. Bubble shapes observed in 0.05% xanthan gum at three different heights

Different bubble shapes at 0.1 m height			
0.1 mL	2 mL	5 mL	10 mL
			
Different bubble shapes at 0.5 m height			
0.1 mL	2 mL	5 mL	10 mL
			
Different bubble shapes at 1 m height			
0.1 mL	2 mL	5 mL	10 mL
			

Table 5. Bubble shapes observed in 0.05% polyacrylamide at three different heights

5.3.3. Bubble shapes in crystal suspension

Re as a function of Eo and E, is illustrated in Figure 27. As expected, Re increases with the increase in Eo and E. The bubbles become more oblate as their size increases. As seen from Table 6, the shapes encountered for larger bubbles (5.0 mL and 10.0 mL) in crystal suspension were mostly ellipsoidal and ellipsoidal cap.

The shape instability was visualised at different heights of the liquid from the still images as are illustrated in Table 6. Usually, the shapes of the bubbles in non-Newtonian liquids are dominated by the magnitudes of inertial, viscous, surface tension, gravity and buoyancy forces (De Kee and Chhabra, 1988). Table 5.5 shows that the bubble volume of 0.1 mL was close to spherical in shape. The 0.1mL bubble was slightly elongated sideways at 0.5 m height and it looked nearly elliptical in shape at 1 m height of the liquid column. On the other hand, the 2.0 mL bubble was continuously distorted, changing into different shapes at different heights, and finally formed into an ellipsoidal shape. This transition from one shape to another is mainly dependent on the rheological properties of the crystal suspension. The shapes reported for larger bubbles (5.0 mL and 10.0 mL) were mainly oblate (flattened from top to bottom end), spherical-capped or ellipsoidal-capped. The larger bubbles (10.0 mL) also differed slightly from the base oblate shape at different heights, and finally looked to be at spherical capped at 1.0 m height.

5.3.4 Shape deformation in crystal suspensions

The bubble deformation parameter D is plotted as a function of the dimensionless bubble diameter in Figure 28. It is experimentally observed that the bubble deformation increases with increase in bubble diameter. As expected, D increases with increase in bubble diameter for other liquids as well. Therefore, Figures for D versus d_{eq} in other liquids are not shown for brevity of the study.

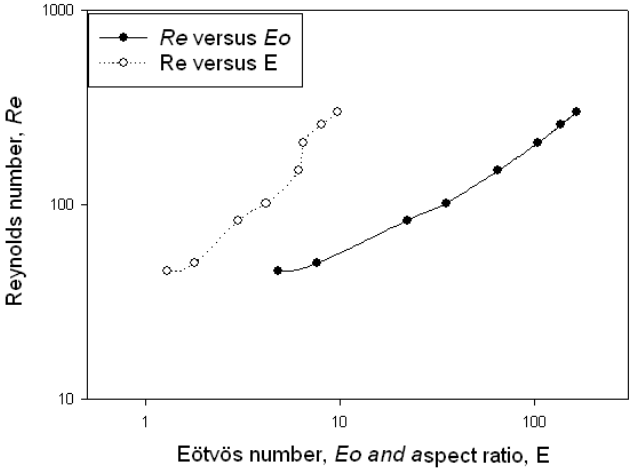

Figure 27. *Re* versus *Eo* and E for crystal suspension

a. Different bubble shapes at 0.1 m height			
0.1 mL	2 mL	5 mL	10 mL
			
b. Different bubble shapes at 0.5 m height			
0.1 mL	2 mL	5 mL	10 mL
			
c. Different bubble shapes at 1 m height			
0.1 mL	2 mL	5 mL	10 mL
			

Table 6. Bubble shapes observed in crystal suspension at three different heights

As seen from Figure 28, this deformation is shown to be minimal in smaller sizes of bubble diameter. However, these bubbles were not fully spherical. As the bubble diameter increases, D increases which is caused by the deformation in bubble shape from close to spherical to the spherical-cap shape bubble observed for the largest bubble of 20 mL (dimensionless equivalent diameter of 31.26).

The bubble shape is assumed to be stable for low We and becomes unstable for larger We. Therefore, the We value is an important parameter to determine the bubble deformation. As shown in Figure 21, the bubble shape deformation normally occurs at the critical Weber number, We_{cr}. The values of We_{cr} for all liquids were calculated and are presented in Figure 21. It is observed from Figure 21 that the We_{cr} must exceeds 7.9 for crystal suspension for bubble shape deformation and elongation and subsequent deformation to occur. As the

bubbles' size increases further, they attain a spherical-cap shape at higher We numbers (We >27.3). The initiation of shape deformation during bubble rise is less rapid in crystal suspension than in water.

All bubble shapes encountered in this research were compared with the available published data and the results are found to be in good agreement with the experimental predictions of Clift *et al.,* (1978); Bhaga and Weber, (1981).

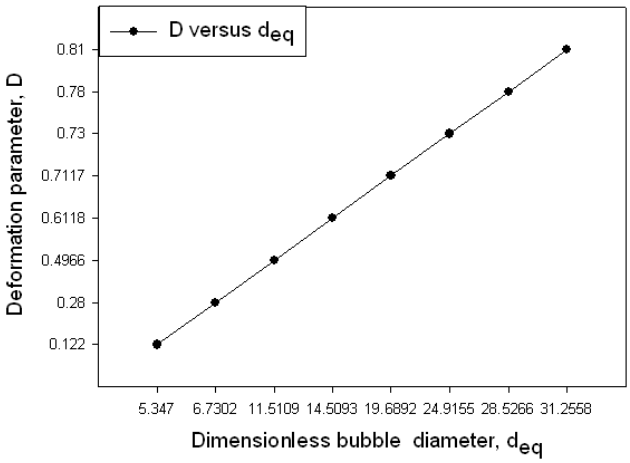

Figure 28. Deformation parameter as a function of dimensionless bubble equivalent diameter

6. Conclusion

A comprehensive comparison of experimental results of the bubble trajectory and shapes are made for water, polymeric solutions and a crystal suspension.

It was seen from this study that the trajectories of bubbles were significantly influenced by the bubble deformations and the surrounding liquid flow, and Re usually controlled the fluid flow regime around the bubble. The influences of Re , We and Mo were seen as important for explaining the bubble trajectories. It was visually observed that the smallest bubbles (5.76 mm) exhibited the most horizontal movement in water and the least in crystal suspension. These smaller bubbles showed a zig-zag trajectory in all fluids. This zig-zag motion was more pronounced in water than in other two fluids.

At intermediate and moderately high Re and We, for bubble sizes of 15.63 mm (2 mL) and 21.21 mm (5.0 mL), path transition occurred and they produced two distinct unstable zigzag and spiral trajectories for all fluids. It was also found that the path transition occurred more rapidly in water than in the other two fluids.

It was observed that larger bubbles (> 21.21 mm) produced a spiral motion in all fluids at very high Re and We . It was also established from experimental observations that larger bubbles (≥ 10.0 mL or 26.84 mm) produced more spiral motion in crystal suspension than in

the other fluids. It was observed that the bubble shapes are greatly dependent on *Re, Eo* and the aspect ratio or eccentricity of bubble, E. The dimensionless numbers such as Mo together with the Eötvös number (Eo) are also used to characterise the shape of bubbles moving in a surrounding fluid.

Generally, spherical, ellipsoidal and spherical cap shapes were observed in all three fluids. Apart from these, other bubble shapes were also encountered in those fluids. A skirted bubble shape was also found in PAM solution. Wobbling bubbles were also reported in water and crystal suspension.

The experimental results substantiated that the path oscillation and the shape deformation of bubble rise was less rapid in crystal suspension than in water.

Author details

N.M.S. Hassan*, M.M.K. Khan and M.G. Rasul
Power and Energy Research Group,
Institute for Resource Industries and Sustainability (IRIS), Faculty of Sciences,
Engineering and Health Central Queensland University, Rockhampton, Queensland, Australia

7. References

Acharya, A., Mashelkar, R. A. and Ulbrecht. J., 1977, Mechanics of bubble motion and deformation in non Newtonian media, Chem. Eng. Sci. 32, 863-872.

Adoua R, Legendre D and Magnaudet J 2009 Reversal of the lift force on an oblate bubble in a weakly viscous linear shear flow *J. Fluid Mech.* 628 23–41.

Adkins, B. G., 1951, Notes on the viscosity of molasses and massecuites, Proc. Qld. Soc. Sugar Cane Technol 18, 43-52.

Awang M., White, E. T., 1976, Effect of crystal on the viscosity of massecuites, Proc. Qld Soc. Sugar Cane Technol., 43, 263-270.

Aybers, N. M., and Tapucu, A., 1969, The motion of gas bubble rising through stagnant liquid, Warme und Stoffubertraguang 2, 118-128.

Bhaga, D. and Weber, M. E., 1981, Bubbles in viscous liquids: shapes, wakes and velocities., Journal of Fluid Mechanics., 105, 61-85.

Bhaga, D., 1976, PhD. Thesis, McGill Univ., Montreal, Canada.

Bhattacharya, S. N., 1997, Rheology fundamentals and measurements, printed at the Royal Melbourne Institute of Technology, Melbourne Australia.

Brenn G, Kolobaric V and Dusrst F 2006 Shape oscillations and path transition of bubbles rising in a model bubble column *Chem. Eng. Sci.* 61 3795–805.

Broadfoot, R. and Miller, K. F., 1990, Rheological studies of massecuites and molasses, International Sugar Journal 92, 107-112.

Broadfoot, R., Miller, K. F. and McLaughlin, R. L., 1998, Rheology of high grade massecuites, Proc. Aust. Soc. Sugar Cane Technol 20, 388 -397.

* Corresponding Author

Bojcic, P., Khan. M. M. K. and Broadfoot, R., 1997, Fitting loss for a power-law viscous fluid at low Reynolds number, Proceedings of the 7th Asian Congress of Fluid mechanics, Chennai, 725-728.

Calderbank, P. H., 1967, Gas absorption from bubbles, The Chem. Engr.,45, CE209, 109-115.

Carreau, P. J., Device, M. and Kapellas, M., 1974, Dynamique des bulles en milieu viscoelastique, Rheol. Acta 13, 477-489.

Chhabra, R. P., 2006, Bubbles, drops, and particles in non-Newtonian fluids, Taylor & Francis Group, CRC Press.

Churchill, S. W., 1989, A theoretical structure and correlating equation for the motion of single bubbles, Chemical Engineering and Processing 26, 269-279.

Clift, R., Grace, J. R. and Weber, M. E., 1978, Bubbles, Drops and Particles, Academic Press, 1978, republished by Dover, 2005.

Davies, R. M. and Taylor, G. I., 1950, The mechanics of large bubbles rising through liquids in tubes, Proc. of Roy. Soc. London, 200 Ser. A, 375-390.

De Kee, D. and Chhabra, R. P., 1988, A photographic study of shapes of bubbles and coalescence in non-Newtonian polymer solutions, Rheol. Acta 27, 656-660.

De Kee, D., Carreau, P. J. and Mordarski, J., 1986, Bubble velocity and coalescence in viscoelastic liquids, Chem. Eng. Sci. 41, 2273-2283.

De Kee, D., Chhabra, R. P. and Dajan, A., 1990, Motion and coalescence of gas bubbles in non-Newtonian polymer solutions, J. Non-Newtonian Fluid Mech. 37, 1-18.

De Kee, D., Chhabra, R. P. and Rodrigue, D., 1996, Hydrodynamic of free-rise bubbles in Non-Newtonian polymer solutions, Handbook of Applied Polymer Processing Technology, 87-123.

De Vries A W G 2001 Path and wake of a rising bubble *PhD Thesis* The University of Twente, the Netherlands.

De Vries, A. W. G., Biesheuvel, A. and Van Wijngaarden, L., 2002, Notes on the path and wake of a gas bubble rising in pure water, Int. Jnl. Multiphase Flow 28, 1823-1835.

Deane, G. B. and Stokes, M. D., 2002, Scale dependence of bubble creation mechanisms in breaking waves, Nature 418, 839-844.

Duineveld, P. C., 1994, Bouncing and coalescence of two bubbles in water, PhD Thesis, University of Twente.

Duineveld, P. C., 1995, The rise velocity and shape of bubbles in pure water at high Reynolds number, Journal of Fluid Mechanics, 292, 325-332.

Ellingsen K and Risso F 2001 On the rise of an ellipsoidal bubble in water: oscillatory paths and liquid induced velocity *J. Fluid Mech.* 440 235–68.

Feng, Z. C. and Leal, L. G., 1997, Nonlinear bubble dynamics, Ann. Rev. Fluid Mech. 29, 201-243.

Fernandes P C, Ern P, Risso F and Magnaudet J 2008 Dynamics of axisymmetric bodies rising along a zigzag path *J. Fluid Mech.* 606 209–23.

Frank, X., Li, H. Z. and Funfschilling, D., 2005, An analytical approach to the rise velocity of periodic bubble trains in non-Newtonian fluids, Eur. Phys. J. E 16, 29-35.

Frank, X., Li, H. Z., Funfschilling, D., Burdin, F. and Ma, Y., 2003, Bubble motion in non-Newtonian fluids and suspensions", Can J Chem Eng., 81:483–490.

Grace, J. R. and Wairegi, T., 1986, Properties and characteristics of drops and bubbles, Encyclopedia of. Fluid Mech., 3, 43-57.

Grace, J. R., 1973, Shapes and velocities of bubbles rising in infinite liquids, Trans. Inst. Chem. Engg. 51, 116-120.

Grace, J. R., Wairegi, T. and Nguyen, T. H., 1976, Shapes and velocities of single drops and. through immiscible liquids, Trans. Inst. Chem. Eng. 54, 167-173.

Haberman, W. L. and Morton, R. K., 1954, An experimental study of bubbles moving in liquids, Trans ASCE 2799, 227-252.

Hartunian, R. A. and Sears, W. R., 1957, On the instability of small gas bubbles moving uniformly in various liquids, Journal of Fluid Mech. 378, 19-70.

Hassan, N. M. S., Khan, M. M. K. and Rasul, M. G., 2007a, Characteristics of air bubble rising in low concentration polymer solutions, WSEAS TRANSACTIONS on FLUID Mechanics, ISSN: 1790-5087, 2 (3), 53-60.

Hassan, N. M. S., Khan, M. M. K., Rasul, M. G. and Rackemann, D. W., 2007b, An experimental study of bubble rise characteristics in non–Newtonian (power-law) fluids, Proceedings of the 16th Australasian Fluid Mechanics Conference, Gold Coast, Australia, 1315-1320.

Hassan, N. M. S., Khan, M. M. K. and Rasul, M. G., 2008a, An investigation of bubble trajectory and drag co-efficient in water and non-Newtonian fluids, WSEAS Transactions on Fluid Mechanics, Special issue: Sustainable Energy and Environmental Fluid Mechanics, ISSN: 1790-5087, 3(3), 261 -270.

Hassan, N. M. S., Khan, M. M. K, Rasul, M. G. and Rackemann, D. W. 2008b, An Experimental investigation of bubble rise characteristics in a crystal suspended non – Newtonian Fluid, Proceedings of the XVth International Congress on Rheology. 80th Annual Meeting, American Institute of Physics (AIP), Monterey, California, USA, ISBN 978-07354-0550-9, 743-745.

Hassan, N. M. S., Khan, M. M. K and Rasul, M. G., 2008c, Air bubble trajectories in polymeric Solutions and crystal Suspensions, Proceedings of the 4th BSME-ASME International Conference on Thermal Engineering, Dhaka, Bangladesh, ISBN 984-300-002844-0, 970- 975.

Hassan, N. M. S., Khan, M. M. K and Rasul, M. G., 2010a, Modelling and experimental study of bubble trajectory in non-Newtonian crystal suspension, Fluid Dynamics Research, IOP Publishing, 42, 065502.

Hassan, N. M. S., Khan, M. M. K., Rasul, M. G. and Rackemann, D. W., 2010b, Bubble rise velocity and trajectory in xanthan gum crystal suspension, Applied Rheology, International Journal, 20, 65102.

Hassan, N. M. S., 2011, Bubble rise phenomena in various non-Newtonian Fluids, PhD Thesis, Central Queensland University, Australia.

Kabir, M. A., Slater, A. R., Khan, M. M. K. and Rackemann, D., 2006, Characteristics of bubble rise in water and polyacrylamide solutions, International Journal of Mechanical and Materials Engineering, 64-69.

Kulkarni, A. A. and Joshi, J. B., 2005, Bubble formation and bubble rise velocity in gas-liquid systems: A. review, Ind. Eng. Chem. Res., 44, 5873-5931.

Lima Ochoterena, R. and Zenit, R., 2003, Visualization of the flow around a bubble moving in a low viscosity liquid, Revista Mexicana De Fisica 49, 348-352.

Maxworthy, T., Gnann, C., Kurten, M. and Durst, F., 1996, Experiments on the rise of air bubbles in clean viscous liquids. J. Fluid Mech. 321, 421-441.

Miyahara, T. and Yamanaka, S., 1993, Mechanics of motion and deformation of a single bubble rising through quiescent highly viscous Newtonian and non-Newtonian Media, Journal of Chemical Engineering of Japan, 26 (3), 297-302.

Magnaudet J and Eames I 2000 The motion of high-reynolds-number bubbles in inhomogeneous flows *Annu. Rev.Fluid Mech.* 32 659–708.

Mougin, G. and Magnaudet, J., 2002, Path instability of a rising bubble. Phys. Rev. Lett. 88 (2002), paper number 014502.

Mougin G and Magnaudet J 2006 Wake-induced forces and torques on a zigzagging/spiralling bubble J. Fluid Mech. 56 7185–94.

Munson, B. R., Young, D. F. and Okiishi, T. H., 2009, Fundamentals of Fluid Mechanics, 6th Edition, John Wiley & Sons, Inc.

Ness, J. N., 1983, On the measurement of massecuite flow properties, Proc. Int. Soc. Sugar Cane Technol 18, 1295-1303.

Nezhad, Hazi, A., 2008, Materials science experimentations of raw materials, intermediates and final products in the sugar beet manufacturing process, Dr.-Eng. Thesis, The Technical University of Berlin.

Rackemann, D. W., 2005, Evaluation of circulation and heat transfer in calandria tubes of crystallisation vacuum pans, M.Sc. Eng. Thesis, James Cook University.

Saffman, P. G., 1956, On the rise of small air bubbles in water, Journal of Fluid Mechanics, Digital Archive, 1: 249-275.

Shew, W. L., and Pinton, J. F., 2006, Viscoelastic effects on the dynamics of a rising bubble, J. Stat. Mech., Online at stacks.iop.org/JSTAT/2006/P01009, doi: 10.1088/1742-5468/2006/01/P01009.

Tadaki, T. and Maeda, S., 1961, On the shape and velocity of single air bubbles rising in various liquids, Chem. Eng. (Tokyo), 25, 254.

Tsuge, H. and Hibino, S. I., 1997, The onset conditions of oscillatory motion of single gas bubbles rising in various liquids, Journal of Chemical Engineering of Japan 10, 66-68.

Wegener P P and Parlange J Y 1973 Spherical-cap bubbles *Annu. Rev. Fluid Mech.* 5 680–9

Whyte, D. S., Davidson, M. R., Carnie, S. and Rudman, M. J., 2000, Calculation of droplet deformation at intermediate Reynolds number using a volume of fluid technique, ANZIAM Journal 42, C1520-C1535.

Yang B 2006 Numerical studies of single gas and vapor bubble flows *PhD Thesis* The John Hopkins University, Baltimore, MD.

Yang B and Prosperetti A 2007 Linear stability of the flow past a spheroidal bubble *J. Fluid Mech.* 582 53–78.

Yoshida, S. and Manasseh, R., 1997, Trajectories of rising bubbles, 16th Japanese Multiphase Flow Symposium, Touha, Hokkaido.
www.wseas.us/e library/transactions/fluid/2008/MGR-08.pdf

Zheng, Li and Yapa, P. D., 2000, Buoyant velocity of spherical and non-spherical bubbles/droplets, Journal of Hydraulic Engineering, 126(1), 852-854.

Zenit R and Magnaudet J 2008 Path instability of rising spheroidal air bubbles: a shape controlled process *Phys. Fluids* 20 1.

Zenit R and Magnaudet J 2009 Measurements of the stream wise vorticity in the wake of an oscillating bubble *Int. J. Multiph. Flow* 35 195–203.